CODEN [USA]: IAJPBB ISSN: 2349-7750

INDO AMERICAN JOURNAL OF
PHARMACEUTICALSCIENCES

http://doi.org/10.5281/zenodo.893297

Available online at: http://www.iajps.com Research Article

3D-QSAR STUDIES OF INDENOPYRAZOLE AS CDK4 INHIBITORS WITH COMFA AND COMSIA METHODS

Md. Muzaffar-ur-Rehman*[1], Shravan Kumar Gunda[1], Leander Corrie[2], Bejjenki Pavan Kumar[3]

[1]Department of bioinformatics, Osmania University, Hyderabad, Telangana-50007, India
[2]Department of pharmaceutics, G. Pulla Reddy College of Pharmacy, Mehdipatnam, Hyderabad, Telangana-500028, India.
[3]Department of pharmaceutics, St. Mary's college of pharmacy, secunderabad, pin: 500025, Telangana, India.

Abstract:
Three-dimensional quantitative structure–activity relationship (3D-QSAR) studies were performed for a series of indenopyrazole inhibitors using comparative molecular field analysis (CoMFA) and comparative molecular similarity indices analysis (CoMSIA) techniques. A training set containing 69 molecules served to establish the models. The optimum CoMFA and CoMSIA models obtained for the training set were all statistically significant with cross-validated coefficients (q^2) of 0.845 and 0.763 and conventional coefficients (r^2) of 0.946 and 0.952, respectively. The predictive capacities of both models were successfully validated by calculating a test set of 24 molecules that were not included in the training set. The CoMFA and CoMSIA field contour maps agree well with the structural characteristics of the binding pocket of CDK4 inhibitor, which suggests that the 3D-QSAR models constructed in this paper can be used to guide the development of novel indenopyrazole inhibitors of CDK4 receptor.

Keywords: *Indenopyrazole derivatives, Test set, Training set, CoMFA, CoMSIA*

Corresponding author:
Md. Muzaffar-ur-Rehman,
17-17/2, Kamala Nagar, Medipally,
Hyderabad, Telangana, India-500098
Email id: m.muzaffar687@gmail.com
Contact no: 8686294437

QR code

Please cite this article in press as Md. Muzaffar-ur-Rehman et al, ***3D-QSAR Studies of Indenopyrazole as CDK4 Inhibitors with CoMFA and CoMSIA Methods****, Indo Am. J. P. Sci, 2017; 4(09).*

INTRODUTION:

Introduction to target protein (2w96) and its role:

Cyclin dependent kinases (CDKs) along with cyclin regulatory subunits are the key regulatory group of protein kinases which regulate different stages of the eukaryotic cell cycle [1] [2]. CDKs are also involved in the control of gene transcription, the processes that integrate extracellular and intracellular signals for the coordination of the cell cycle in response to environmental change, and apoptosis [2] [5] [6]. CDKs are usually activated via phosphorylation of specific threonine residues by the CDK-activating kinase and binding to a cyclin protein. CDK4 plays a central role in the regulation of the G0–G1 phase of the cell and is required for the G1/S phase transition. This depends on extracellular signals and cell-intrinsic information, which determine CDK reactivation after the previous cell cycle[3].Stimulation of quiescent cells with mitogens and growth factors induces expression of D-type cyclins (D1, D2, D3 in mammals) and activation of CDK4 or CDK6 (together: CDK4/6)[4] . CDK4/6-cyclin D is responsible for limited phosphorylation of the retinoblastoma tumor suppressor (Rb) protein. This phosphorylation is thought to weaken the interaction between pRb and the heterodimeric transcription factor E2F/DP (together referred to as E2F). pRb is a negative regulator of the E2F family of transcription factors[7], hence phosphorylation of pRb results in the release of transcription factors which activate the expression of the S-phase genes. This process enables the cell to pass through the restriction point and results in the onset of the S-phase [7] [8]. As the repression of activating E2Fs by pRb is reduced, it allows initial transcription of E2F-dependent genes that include cyclin E and other cell cycle genes. Subsequent activation of CDK2-cyclin E leads to further phosphorylation and inactivation of pRb, release of E2F, and full commitment to S-phase entry [5]. Cell cycle regulators are frequently mutated in human cancers and due to their central role in G1 regulation CDKs offer attractive targets for therapeutic inhibition [9] [10]. Phosphorylation by CDK-cyclin complexes counteracts the binding between retinoblastoma tumor suppressor (Rb) family proteins and E2F transcription factors, thereby allowing transcriptional activation of S-phase genes. In addition to pRb-mediated transcriptional repression, several other levels of control counteract progression from G1 into S-phase. This includes members of 2 different families of CDK inhibitory proteins (CKIs) that associate with CDKs [11]. CKIs of the INK4 protein family, such as p16INK4A, bind specifically to CDK4/6 kinases and prevent their interaction with D-type cyclins. In contrast, CKIs of the CIP/KIP family associate with CDK-cyclin complexes and block their activity. The CIP/KIP family consists of p21Cip1, p27Kip1, and p57Kip2 and is particularly important for temporal control of CDK2-cyclin E. Proteins of both CKI families contributes to cell cycle exit and show increased expression in differentiating cells. The importance of CKIs is further underscored by the functional inactivation of p16INK4A in a wide variety of human cancers [12]. Entry into the cell cycle is also controlled by ubiquitin-dependent protein degradation. This is primarily regulated at the level of substrate recognition by E3 ubiquitin ligases. E3 ligases with important functions in G1/S inhibition are the Anaphase Promoting Complex/Cyclosome (APC/C) in association with the FZR1/Cdh1 coactivator, and Skp1, Cullin, F-box factor (SCF) complexes. SCF in complex with the Fbw7 substrate-recognition factor targets cyclin E for degradation and inhibits cell cycle progression. In contrast, SCF in association with Skp2 directs the destruction of p21Cip1 and p27Kip1 and promotes cell cycle entry.

The work of Yu et al. [13] and Landis et al.[14] suggests that inhibition of CDK4 might benefit patients with ErbB-2 initiated breast cancers[10]. The CDK4/CyclinD1 complex as an anti-cancer drug target has been further validated in MCF-7 breast cancer cells [15] [16].

Introduction to Drug (Indenopyrazole derivatives)

Indenopyrazole framework is a three-ringed heterocyclic structure consisting of a benzene ring, a central 5-membered ring and a pyrazole moiety as shown in the figure 1. The pyrazole portion may tautomerize and an indenopyrazole could exist in two tautomeric forms shown in figure no.2 [17]. Indenopyrazoles have shown diverse biological activities, such as anti-psychotic, anti-mycobacterial [18], and anticancer [16]. In recent years, indenopyrazoles are widely used as the “privileged structure” in the design of anticancer agents targeting multiple tumor target**s.** The derivatives are shown in the table 1.

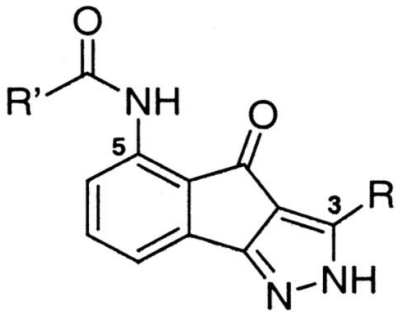

Fig 1: Structure of Indenopyrazole

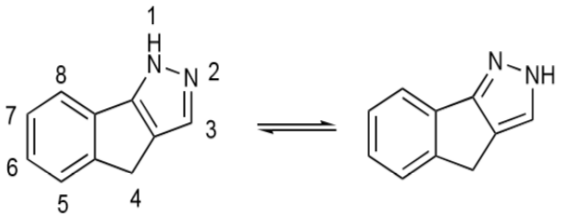

Fig 2: Tautomeric Form of Indenopyrazole

Table 1: Derivatives of Indenopyrazole Having Different Substituents

S.no	R1	X	R2
1	$(CH_3)_2$	CH	–Ph-4-OMe
2	$(CH_3)_3$	C	–Ph-4-OMe
3	$(Me)_2$ N-	CH_2	–Ph-4-OMe
4[a,b]	Morpholine-4-yl	CH_2	–Ph-4-OMe
5	Piperazin-1-yl	CH_2	–Ph-4-OMe
6	Ethyl-NH	CH_2	–Ph-4-OMe
7[b]	N-methyl piperazine	CH_2	–Ph-4-OMe
8	4-Aminomethylpiperidine	CH_2	–Ph-4-OMe
9[a]	4-Amidopiperidine	CH_2	–Ph-4-OMe
10	4-Hydroxylmethylpiperidine	CH_2	–Ph-4-OMe
11[b]	4-Amidopiperazine	CH_2	–Ph-4-OMe
12[a]	4-Amidinopiperazine	CH_2	–Ph-4-OMe
13[b]	H	CH_2	–Ph-4-OMe
14	Benzyl	NH	–Ph-4-OMe
15	Phenyl	NH	–Ph-4-OMe
16	n-Butyl	NH	–Ph-4-OMe
17[b]	$(Me)_2$ NNH	NH	–Ph-4-OMe
18[a]	4-Methylpiperazine	NH	–Ph-4-OMe
19[b]	Morpholine-4-yl	NH	–Ph-4-OMe
20[b]	Piperidin-1-yl	NH	–Ph-4-OMe
21	Pyrrolidine-1-yl	NH	–Ph-4-OMe
22	H	CH_2	–Ph-4-OMe
23	H	CH_2	–Ph-4-OMe
24	H	CH_2	–Ph-4-Et
25	H	CH_2	–Ph-4-n-Pr
26[b]	H	CH_2	–Ph-4-OH
27	–Ph-4-NH_2	CH_2	–Ph-4-OMe
28	H	CH_2	–Ph-4-NMe_2
29	H	CH_2	–Ph-4piperidino
30	H	CH_2	–Ph-4-morpholino
31[a]	H	CH_2	–Ph-4-SMe
32[a,b]	Morpholino	CH_2	–Ph-4-NMe_2
33	4-(OH)piperidine-1-yl	CH_2	–Ph-4-NMe_2

Continue.....

34	4-(Aminomethyl) piperidin-1-yl	CH_2	–Ph-4-NMe_2
35[b]	N-Methylpiperazin-1-yl	CH_2	–Ph-4-NMe_2
36	Morpholino	CH_2	–Ph-4-morpholino
37	4-(OH) piperidine-1-yl	CH_2	–Ph-4-morpholino
38	4-(Aminomethyl) piperidin-1-yl	CH_2	–Ph-4-morpholino
39	H	NH	3-thienyl
40[a,b]	N-Methylpiperazin-1-yl	CH_2	–Ph-4-morpholino
41	4-(Aminomethyl) piperidin-1-yl	CH_2	Et
42	4-(Aminomethyl) piperidin-1-yl	CH_2	Cyclopropyl
43	4-(Aminomethyl) piperidin-1-yl	CH_2	Cyclohexyl
44	H	NH	Cyclopropyl
45	H	CH_2	4-Pyridyl
46	H	CH_2	2-Thienyl
47[a,b]	H	NH	2-Thienyl
48	H	NH	2-Thienyl,3-OMe
49	H	NH	2-Thienyl,5-Me
50[a,b]	H	NH	2-Furanyl
51	H	NH	2-Thienyl,5-CO_2 Et
52	H	NH	3-Thienyl,5-Cl
53	H	NH	3-Pyrrolyl,1-Me
54[b]	Dimethylamino	NH	2-Thienyl
55	Dimethylamino	NH	5-(OMe) thien-2-yl
56	Dimethylamino	NH	5-(Me) thien-2-yl
57	Dimethylamino	NH	5-(CO_2 Et) thien-2-yl
58[a,b]	Dimethylamino	NH	3-Thienyl
59[a]	Dimethylamino	NH	5-(Cl) thien-3-yl
60	Dimethylamino	NH	2,5-(Di-Me) thien-3-yl
61[a]	Dimethylamino	NH	Furan-2-yl
62	Dimethylamino	NH	2,4-(Di-Me)thiazol-5-yl
63[a]	Morpholine-4-yl	NH	5-(Me) thien-2-yl
64	Morpholine-4-yl	NH	5-(CO_2 Et) thien-2-yl
65	Morpholine-4-yl	NH	5-(Cl) thien-3-yl
66	4-(Methyl)piperazin-1-yl	NH	5-(CO_2 Et) thien-2-yl
67	4-(Aminomethyl) piperidin-1-yl	NH	Isopropyl
68	4-(Methyl)piperazin-1-yl	NH	2,5-(Di-Me) thien-3-yl
69	4-(Methyl)piperazin-1-yl	NH	2,4-(Di-Me)thiazol-5-yl
70	$(Me)_2$ CHCONH–	NH	–Ph-4-OMe
71[a]	4-(OH)Ph(CH_2)$_2$ CONH–	NH	–Ph-4-OMe
72	4-(OMe)PhCONH–	NH	–Ph-4-OMe
73	3-(NO_2)PhCONH–	NH	–Ph-4-OMe
74	3,4,5-(Tri-OMe)PhCONH–	NH	–Ph-4-OMe
75	3-(Me)PhCONH–	NH	–Ph-4-OMe
76	3,4-(Di-OMe)PhCONH–	NH	–Ph-4-OMe
77	(4-OH,3-NH_2) PhCONH–	NH	–Ph-4-OMe

Continue.....

78[a,b]	2,5-(Di-Cl)PhCONH–	NH	–Ph-4-OMe
79	3,4-(Di-OH)PhCONH–	NH	–Ph-4-OMe
80	3,5-(Di-NH_2)PhCONH–	NH	–Ph-4-OMe
81[a]	MeOCONH–	NH	–Ph-4-OMe
82	2-(OH)PhCONH–	NH	–Ph-4-OMe
83	Naphthalen-2-yl CONH–	NH	–Ph-4-OMe
84[a,b]	BnCONH–	NH	–Ph-4-OMe
85	PhCONH–	NH	–Ph-4-OMe
86[a]	4-PyrridylCONH–	NH	–Ph-4-OMe
87	3-PyrridylCONH–	NH	–Ph-4-OMe
88[a,b]	MeCONH–	NH	–Ph-4-OMe
89	4-(OH)PHCONH–	NH	–Ph-4-OMe
90[a,b]	H_2 NCOCONH–	NH	–Ph-4-OMe
91[b]	3-(NH_2)PhCONH–	NH	–Ph-4-OMe
92	2,4-(Di-OH)PhCONH–	NH	–Ph-4-OMe
93	4-NH_2 PhCONH–	NH	–Ph-4-OMe

METHODOLOGY:

Geometry optimization:

Ninety three cyclic dependent kinase 4 inhibitor (cdk4) analogues reported to be efficient cdk4 blockers were chosen for this study. IC_{50} values available in the literature were used to calculate pIC_{50} ($-\log IC_{50}$) values for all of the 93 compounds. Among those 93 cdk4 inhibitor analogues, compound 2 has the least activity (pIC_{50}= 4.3470) and compound 88 (pIC_{50}= 8.3010) is highly active. Chemical structures of these 93 cdk4 inhibitor analogues were drawn and were geometrically optimized on SYBYL using default parameters and convergence criterion of 0.001 kcal/mol. The energy minimization of these 93 compounds was performed using tripos force field and the Gasteiger-Huckel charges using a distance-dependent dielectric and powell conjugate gradient algorithm with the convergence criterion of 0.05 kcal/mol. Further geometric optimization of these cdk4 inhibitors was performed.

Alignment: In 3D-QSAR studies, a geometric similarity has to be established between the structures, so optimized structures were aligned on the most active molecule from the set as a template. This adjusts the geometry of the molecules in such a way that the steric and electrostatic fields of the molecules match the with fields of the template molecule.

3D- QSAR- CoMFA and CoMSIA and contour analyses

Three-dimensional quantitative structure activity relationship (QSAR) studies that include comparative molecular field analysis (CoMFA) and molecular similarity indices in comparative analysis (CoMSIA) methods were conducted on these 93 cdk4 inhibitors to assess their potential as cdk blockers. CoMFA employs tripos force field with a distance-dependent, dielectric constant in all interactions in a regularly spaced (2×10^{-10} m) grid taking a sp3 carbon atom as steric probe and a +1 charge as electrostatic probe. The cut-off was set to 30 Kcal/mol. CoMSIA uses a Gaussian-type distance-dependent dielectric constant to minimize changes in atomic positions and charge potentials at the grids.

CoMSIA calculates using a C+ probe atom with a radius of 1×10^{-10} m placed at a regular grid spacing of 2×10^{-10} m to enclose all the binding conformations of the inhibitors. Using default parameters, steric, electrostatic, and hydrophobic field parameters were calculated. The steric filed contribution is denoted by the third power of the atomic radii of the atoms and electrostatic properties were given as atomic charges that were obtained from FlexX docking.

Hydrophobicity was calculated as atom dependent parameter and an approximately 4Å lattice grid was used to include all the binding conformations of the inhibitors. In this study, similarity indices were computed using a probe atom (Wprobe,k) with charge +1, radius 1Å, hydrophobicity +1, and attenuation factor, a, of 0.3 for the Gaussian type distance. The statistical analysis for the CoMSIA analyses was similar to CoMFA.

The pIC_{50} data will couple 3-log units offering a wide and similar set of data for 3D-QSAR analysis. Compounds were divided into test and training sets in 1:3 ratio to improve the predictability of the 3D-QSAR models. Cross-validation and partial least score (PLS) analyses were used where the cross-validated coefficient (q^2), leaving optimal number of components and lowest standard error of prediction, was considered for the accuracy determination of the predicted models.

The reliability of a 3D-QSAR model depends on the activity prediction ability of the model. Pearson's correlation coefficient, r^2, is the squared correlation coefficient that measures the precision of adjustment for the fitted values to the observed ones. In cross-validation, the outcome of the LOO procedure is a cross-validated correlation coefficient (r^2, cv or q^2) that indicates the robustness and predictive ability of the model. The cross-validated correlation coefficient, q^2, is regarded as a measure of internal consistency of the derived model.

RESULTS AND DISCUSSION:

CoMFA and CoMSIA results for CDK4 inhibitors:

The CoMFA method was used for deriving a 3D-QSAR model for 93 cdk4 inhibitors, which are reported to inhibit cdk4 emzyme. The molecules were aligned, one over the other, to generate a basic common moiety. The image below shows the alignment of 93 molecules and the common-core ring. The leave-one-out partial least-squares (PLS) analysis of the obtained model yielded a high, cross-validated q^2-value of 0.845 (five components) and a non-cross-validated correlation-coefficient, r^2, of 0.946. This correlation coefficient suggests the model to be reliable and accurate.

The alignment:

Table 2 and Table 3 lists CoMFA and CoMSIA experimental activities, predicted activities, and residual values of the training set and test set respectively. CoMFA and CoMSIA 3D-QSAR models were generated using cdk4 inhibitor analogues. Upon analyzing IC_{50} and pIC_{50} values, compound 12 was the least active compound, and a compound 88 was the most active compound.

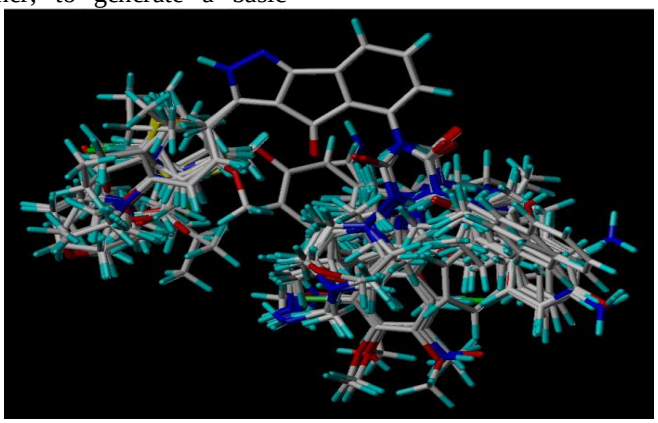

Fig 3: Show the Aligned Structure of All 93 CDK4 Inhibitors and the Common Core Ring Present In All Those Molecules, thus aiding QSAR Studies.

Table 2: CoMFA and CoMSIA PREDICTED and Residual Values for the Training Data Set.

TRAINING SET					
		CoMFA		CoMSIA	
C.NO	PIC50	PREDICTED	RESIDUAL	PREDICTED	RESIDUAL
C10	7.086	7.216	-0.13	7.201	-0.115
C11	7.194	7.413	-0.219	7.611	-0.417
C12	7.585	7.177	0.408	7.081	0.504
C13	6.347	6.219	0.128	6.372	-0.025
C14	6.512	7.55	-1.038	7.38	-0.868
C15	6.057	6.77	-0.713	6.482	-0.425
C18	8.046	7.767	0.279	7.747	0.299
C19	7.921	7.568	0.353	8.089	-0.168
C20	7.921	7.636	0.285	7.481	0.44
C22	6.076	5.918	0.158	6.046	0.03
C23	6.31	5.871	0.439	6.004	0.306
C24	6.194	6.109	0.085	6.026	0.168
C25	5.721	6.324	-0.603	6.302	-0.581
C26	5.638	5.987	-0.349	5.923	-0.285
C27	6.319	6.491	-0.172	6.449	-0.13

Continue.....

C28	6.509	6.107	0.402	6.164	0.345
C29	6.167	6.072	0.095	6.401	-0.234
C3	6.046	6.477	-0.431	6.494	-0.448
C30	6.065	6.116	-0.051	6.07	-0.005
C31	6.468	5.965	0.503	5.793	0.675
C32	6.959	7.175	-0.216	7.236	-0.277
C33	7.301	7.348	-0.047	7.668	-0.367
C34	8.155	7.521	0.634	7.427	0.728
C35	7.26	7.064	0.196	7.228	0.032
C36	6.921	7.078	-0.157	7.102	-0.181
C37	6.959	7.074	-0.115	6.843	0.116
C4	6.71	6.643	0.067	6.799	-0.089
C41	5.886	6.465	-0.579	6.488	-0.602
C42	6.366	6.248	0.118	6.069	0.297
C43	6.444	6.31	0.134	6.008	0.436
C44	5.854	5.626	0.228	6.67	-0.816
C45	5.886	6.139	-0.253	5.789	0.097
C46	5.347	5.624	-0.277	5.928	-0.581
C5	6.947	6.653	0.294	6.384	0.563
C51	6.523	6.624	-0.101	6.555	-0.032
C54	6.468	6.458	0.01	6.322	0.146
C55	7.076	6.917	0.159	6.589	0.487
C57	6.733	6.795	-0.062	7.022	-0.289
C6	6.038	6.516	-0.478	6.395	-0.357
C60	6.288	6.47	-0.182	6.644	-0.356
C61	6.197	6.353	-0.156	6.548	-0.351
C62	6.824	6.527	0.297	6.706	0.118
C63	7.638	7.546	0.092	7.632	0.006
C64	7.523	7.226	0.297	7.303	0.22
C66	7.523	7.296	0.227	6.745	0.778
C68	7.046	7.197	-0.151	7.397	-0.351
C69	7.337	7.252	0.085	7.329	0.008
C7	6.903	6.882	0.021	6.75	0.153
C70	8.187	7.803	0.384	7.026	1.161
C71	7.959	7.984	-0.025	8.146	-0.187
C72	8	7.967	0.033	7.934	0.066
C73	8.155	7.922	0.233	7.903	0.252
C74	8.155	8.169	-0.014	7.99	0.165
C75	7.62	8.031	-0.411	8	-0.38
C76	8.155	7.986	0.169	7.923	0.232
C77	7.553	7.943	-0.39	8.02	-0.467
C78	8.301	7.816	0.485	7.798	0.503
C79	7.796	7.99	-0.194	7.85	-0.054
C80	8.097	8.023	0.074	7.46	0.637

Continue.....

C81	7.222	7.676	-0.454	7.91	-0.688
C82	7.886	7.358	0.528	7.602	0.284
C83	7.569	7.555	0.014	7.707	-0.138
C84	8.155	7.854	0.301	7.542	0.613
C85	8.046	7.959	0.087	7.977	0.069
C86	8.046	7.981	0.065	7.899	0.147
C88	8.301	7.604	0.697	7.876	0.425
C9	7.119	6.857	0.262	7.022	0.097
C90	8.155	8.052	0.103	8.168	-0.013
C91	7.921	8.09	-0.169	7.935	-0.014
C92	8	8.049	-0.049	8.137	-0.137

Table 3: COoMFA and CoMSIA Values for the Test Data Set

TEST SET					
		CoMFA		CoMSIA	
C.NO	PIC50	PREDICTED	RESIDUAL	PREDICTED	RESIDUAL
C1	4.456	7	-2.544	5.43	-0.974
C16	6.108	7.22	-1.112	6.2	-0.092
C17	7.678	6.96	0.718	7.76	-0.082
C2	4.347	6.47	-2.123	5.25	-0.903
C21	7.921	7.24	0.681	7.77	0.151
C38	7.745	7.05	0.695	7.39	0.355
C39	7.174	5.8	1.374	6.85	0.324
C40	6.721	7.3	-0.579	7.21	-0.489
C47	6.824	5.28	1.544	6.83	-0.006
C48	6.456	5.68	0.776	6.55	-0.094
C49	7.276	5.48	1.796	6.92	0.356
C50	6.076	5.28	0.796	6.17	-0.094
C52	7.244	5.8	1.444	6.99	0.254
C53	6.886	6.08	0.806	6.91	-0.024
C56	7.091	6.87	0.221	7.1	-0.009
C58	6.971	6.19	0.781	7.26	-0.289
C59	7.678	6.23	1.448	7.31	0.368
C65	8.155	7.39	0.765	8.01	0.145
C67	6.468	7.22	-0.752	6.91	-0.442
C8	7.699	6.9	0.799	7.24	0.459
C87	7.244	8	-0.756	7.51	-0.266
C89	6.62	7.76	-1.14	7.41	-0.79
C93	7.18	7.96	-0.78	7.34	-0.16
C94	5.939	7.07	-1.131	7.07	-1.131

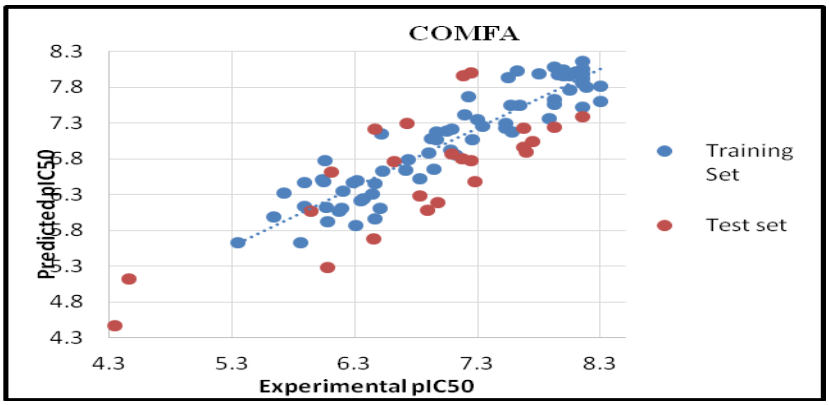

Fig 4: The Graphical Representation of CoMFA Studies Done Under Qsar Which Include Test Set And Training Set Respectively.

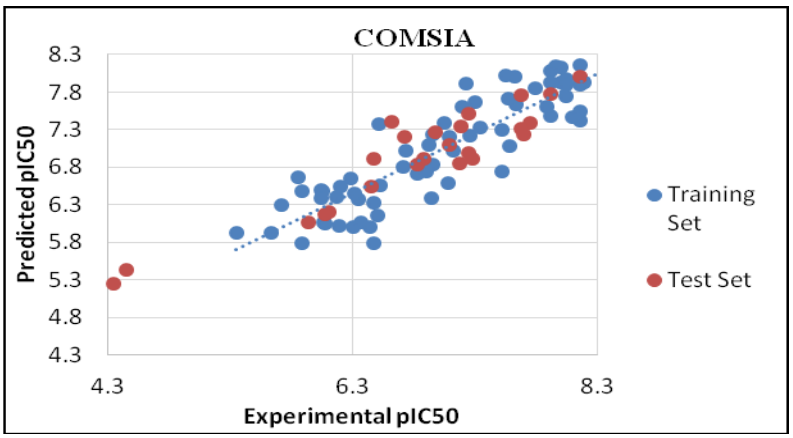

Fig 5: Show The Graphical Representation of CoMSIA Studies Done Under QSAR Which Include Test Set and Training Set Respectively.

Table 4: Shows the PLS Statistics of COMFA and COMSIA, 3D-QSAR Models.

	COMFA	COMSIA
q^2	0.845	0.763
r^2	0.946	0.952
STANDARD ERROR OF ESTIMATE	0.199	0.190
F VALUE	223.070	206.549
STEARIC	71.8%	23.2%
ELECTROSTATIC	28.2%	18.2%
DONAR	-	22.39%
ACCEPTOR	-	13.9%
HYDROPHOBIC	-	21.8%
CROSS VALIDATION	0.822	0.747

BOOTSTRAP				
	MEAN	STANDARD DEVIATION	MEAN	STANDARD DEVIATION
STANDARD ERROR OF ESTIMATE	0.187	0.087	0.136	0.061
r^2	0.949	0.011	0.975	0.006

CoMFA analysis and statistical validity predict compound 88 to be the most potent and stable CYCLIC DPENDENT KINASE 4(CDK4) INHIBITOR

69 cdk4 inhibitors were used for training set whereas the remaining 24 cdk4 inhibitors were used in test set. The compounds in the test set were chosen manually to ensure that the compounds included possess a broad activity range. The steric and electrostatic field descriptors explain 71.8% and 28.2 % of the variance, respectively (Table 4). Predicted values support the statistical validity of the developed models and correlate with the experimental values, supporting the reliability of predicted CoMFA model (Table 3).

The q^2- LOO-cross-validated correlation coefficient, r^2, non-cross-validated correlation coefficient, n-number of components used in the PLS analysis, SEE-standard error estimation, F-statistic for the analysis values shown demonstrate the accuracy and stability of our model.

CoMSIA analysis demonstrates the accuracy of predicted models

Four major field descriptors: steric, electrostatic, hydrophobic, and hydrogen bond donor fields were used to run the CoMSIA analysis. The CoMSIA analysis demonstrated a cross-validated q^2 of 0.763, a conventional r^2 of 0.952 with a SEE of 0.136, and F value of 206.549 for training set (Table 4). The steric, the electrostatic, hydrophobic field, hydrogen bond donor, and hydrogen bond acceptor field descriptors explain 23.2 %, 18.2 %, 21.8 %, 22.39% and, 13.9 % of the variance, respectively (Table 4). The above results demonstrate that the predicted CoMSIA model is reliable and accurate. These results demonstrate that the CoMFA and CoMSIA models can be reliably used in the design of novel CDK4 inhibitors.

Contour analysis with all the major field descriptors analyzed predict compound 88 to be the most active and stable cdk4 blocker.

Contour map analysis was performed on SYBYL 1.1 to visualize the generated CoMFA and CoMSIA models. During contour map analysis, contour with contribution values of 80% for favored region and 20% for disfavored region were set as the default level.

CoMFA contour maps with steric and electrostatic contours indicate the stability of compound 88 as cdk4 inhibitor

Images of CoMFA steric and electrostatic contours with highest activity (compound 88) is shown in Fig. In Fig.5 of CoMFA – steric interactions in counter maps of cyclic dpendent kinase inhibitor 4(cdk4) with highest activity (compound 88) – the green and yellow polyhedrons indicate regions where increased or decreased steric bulk, respectively, are predicted to enhance activity.

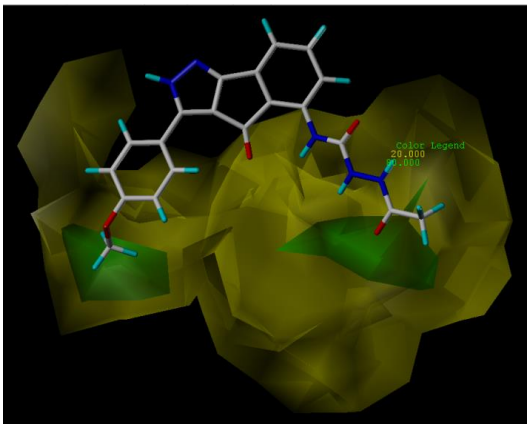

Fig.6: CoMFA Steric Counter Map of Cyclic Dependent Kinase Inhibitor 4(CDK4) With Highest Activity (Compound 88).

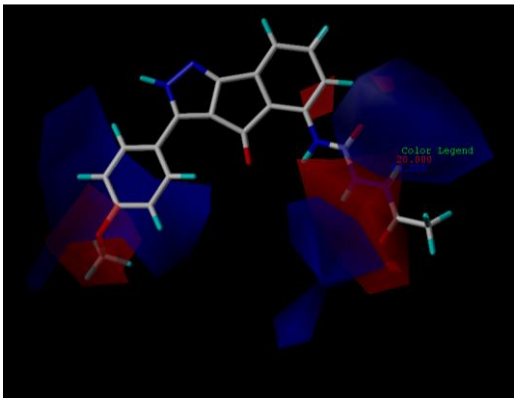

Fig. 7 CoMFA electrostatic counter map of cyclic dpendent kinase inhibitor 4(CDK4) with most activity (compound 88).

The green and yellow polyhedrons indicate regions where increased or decreased steric bulk, respectively, are predicted to enhance activity.

The red and blue polyhedrons indicate regions where higher electron density (negative charge) and lower electron density (partial positive charge), respectively, are predicted to enhance activity.

CoMSIA contour maps CoMFA contour maps with steric, electrostatic, hydrophobic, and hydrogen bond donor and acceptor fields indicate compound 88 to be the most active and stable CDK4 blocker.

The steric, electrostatic, hydrophobic, and hydrogen bond donor and acceptor fields were used to construct the CoMSIA contours maps. The steric and electrostatic contour maps of CoMFA and CoMSIA are almost identical, indicating a similar role. The CoMSIA steric and electrostatic contours maps are shown in fig no:8 (highest activit**y).**

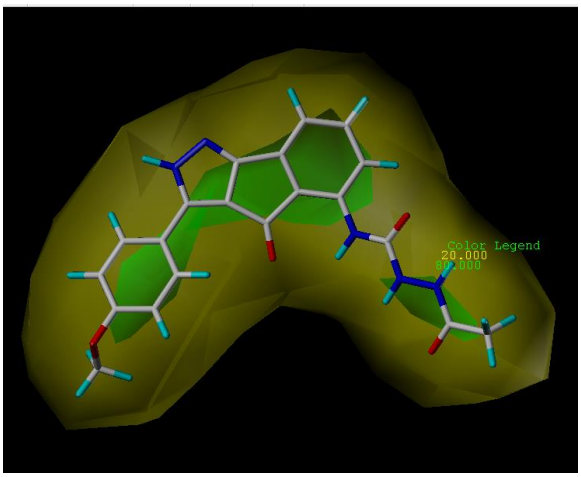

Fig 8: CoMSIA Steric Counter Maps of Cyclic Dependent Kinase Inhibitor 4(CDK4) Having Highest Activity (Compound 88).

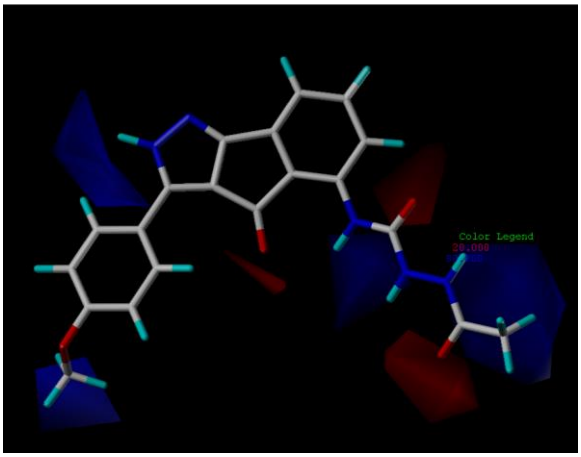

Fig 9: Comsia Electrostatic Counter Maps Of Cyclic Dependent Kinase Inhibitor 4(CDK4) Having Highest Activity (Compound 88).

The green and yellow polyhedrons indicate regions where increased or decreased steric bulk, respectively, are predicted to enhance activity.

The red and blue polyhedrons indicate regions where higher electron density (negative charge) and lower electron density (partial positive charge), respectively, are predicted to enhance activity.

The CoMSIA hydrophobic counter maps of cycic dependent kinase inhibitir4 with highest activity (compound 88) is shown in Fig no:10. The favourable hydrophobic region is represented by white contours, and unfavourable regions are represented by yellow contours. In Fig. 9, CoMSIA hydrophobic contour map of compound 88, yellow contours representing unfavourable regions are seen, indicating the least activity of molecule.

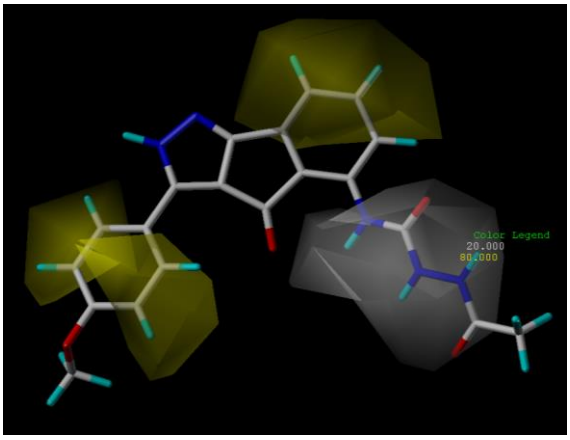

Fig. 10: Comsia Hydrophobic Counter Maps Of Cyclic Dpendent Kinase Inhibitor 4(Cdk4) Having Highest Activity (Compound 88).

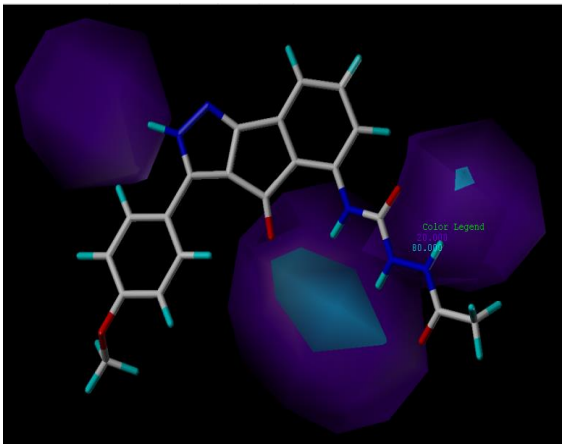

Fig. 11: CoMSIA Hydrogen Donor Of (Hydrogen Bond) Counter Maps of Cyclic Dpendent Kinase Inhibitor 4(CDK4) Having Highest Activity (Compound 88).

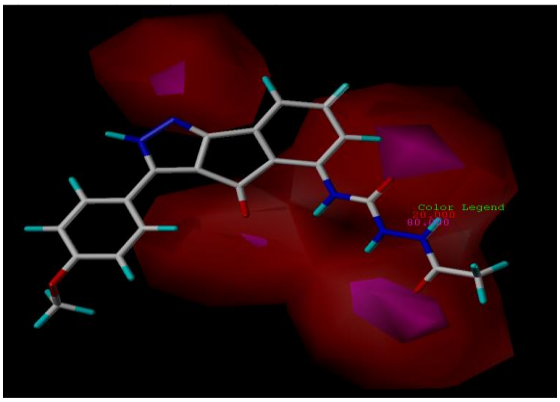

Fig. 12: CoMSIA Active Hydrogen Acceptor Of (Hydrogen Bond) Counter Maps of Cyclic Dependent Kinase Inhibitor 4(CDK4) Having Highest Activity (Compound 88).

Red polyhedron beyond the ligands where a hydrogen bond donor group in the ligand will be favorable for biological activity, and the purple polyhedron represents hydrogen bond acceptor in the ligands unfavorable for bioactivity.

Red polyhedron beyond the ligands where a hydrogen bond donor group in the ligand will be favorable for biological activity, and the purple polyhedron represents hydrogen bond acceptor in the ligands unfavorable for bioactivity.

Molecular Docking:

Protein-ligand docking studies were carried out based on crystal structure of cdk4 in complex with a d-type cyclin(PDB: 2W96 Day, P.J. et al. 2009). Prior to docking all solvent molecules and the co-crystallized ligands was removed from the structure. Molecular docking calculations for the compounds with the proteins were undertaken using Autodock 4.2.5. The grid box parameters were generated with the default selection around the crystallographic ligands and these parameters were utilized to generate the configuration file to run the AutoDock Vina. The receptor structural information required by the program (the pdbqt files) were generated using Pymol with the AutoDock plugin, and the ligand pdbqt files were generated by utilizing scripts included in the Molecular Graphics Laboratory (MGL) tools. Docking was performed to three different molecules with highest, moderate and least active compounds respectively. The binding energy, their kI values and RMSD values are as shown in the table 5:

Table 5: Shows the Details of the Interacting Amino Acids with the Drug

Ligand	Interacting amino acid	Binding energy(ΔG) kCal/Mol	Dissociation constant (kI)	Reference RMSD (Å)
C88	ASN83	-7.33	4.26µm	61.92
C56	SER197	-7.76	2.03 µm	60.24
C12	ILE196	-8.32	797.12nm	60.50

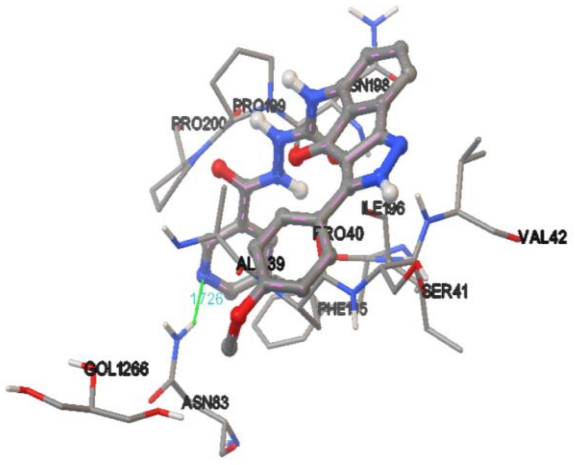

Fig 13: Shows the Docked Image of the Most Active Compound (Compound 88)

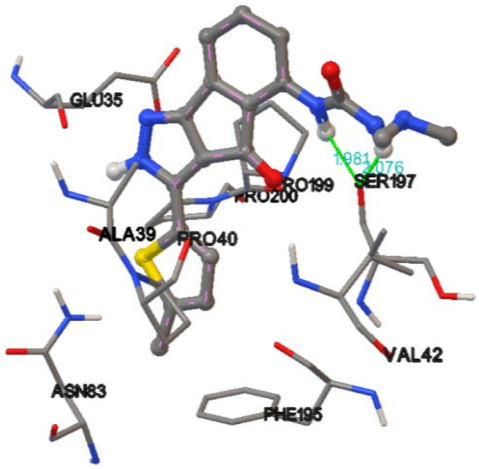

Fig 14: Shows the Docked Image of the Moderate Active Compound (Compound 56)

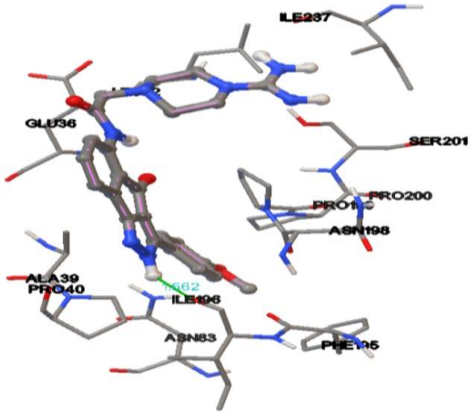

Fig 15: Shows the Docked Image Of The Least Active Compound (Compound 12)

CONCLUSION:

Three-dimensional quantitative structure–activity relationship (3D-QSAR) studies were performed for a series of indenopyrazole inhibitors using comparative molecular field analysis (CoMFA) and comparative molecular similarity indices analysis (CoMSIA) techniques. A training set containing 93 molecules served to establish the models. The optimum CoMFA and CoMSIA models obtained for the training set were all statistically significant with cross-validated coefficients (q^2) of 0.845 and 0.763 and conventional coefficients (r^2) of 0.946 and 0.952, respectively. The predictive capacities of both models were successfully validated by calculating a test set of 24 molecules that were not included in the training set. The dock score of compound 56 is not the highest (the highest dock score was compound 88 with −7.33 KJ/mol) among all the 93 compounds tested in the study, from the Autodock docking interactions and contour map analysis it can be predicted that the amino acid interactions and force fields of compound 56 with 2W96 are critical for rendering this compound potent. Based on the interactions of compound 56 with the active site of 2W96 and force-field interactions we predict that compound 56 can be effectively used in biological systems as a 2w96 inhibitor as it will be potent and stable. Compound 12, being the least active compound, has shown an Auto dock score of −8.32KJ/mol with one interaction. Even though the dock score of compound 12 is considerably high, it can be predicted that this compound is not stable (based on contour map analysis) and that the interactions with the active site of 2W96 is not strong enough to block the pump.

ACKNOWLEDGEMENT

I am highly indebted to the faculty of Osmania University for their guidance and constant supervision as well as for providing necessary facilities to perform the work.

REFERENCES:

1.Shafiq MI, Steinbrecher T, Schmid R. Fascaplysin as a specific inhibitor for CDK4: Insights from molecular modelling. PLoS One. 2012 Aug 14;7(8):e42612.

2.Morgan DO. Cyclin-dependent kinases: engines, clocks, and microprocessors. Annual review of cell and developmental biology. 1997 Nov;13(1):261-91.

3.Spencer SL, Cappell SD, Tsai FC, Overton KW, Wang CL, Meyer T. The proliferation-quiescence decision is controlled by a bifurcation in CDK2 activity at mitotic exit. Cell. 2013 Oct 10;155(2):369-83.

4.Choi YJ, Anders L. Signaling through cyclin D-dependent kinases. Oncogene. 2014 Apr 10;33(15):1890.

5.Malumbres M, Barbacid M. Mammalian cyclin-dependent kinases. Trends in biochemical sciences. 2005 Nov 30;30(11):630-41.

6.Murray AW. Recycling the cell cycle: cyclins revisited. Cell. 2004 Jan 23;116(2):221-34.

7.Sherr CJ. Cancer cell cycles. Science. 1996 Dec 6;274(5293):1672-7.

8.Attwooll C, Denchi EL, Helin K. The E2F family: specific functions and overlapping interests. The EMBO journal. 2004 Dec 8;23(24):4709-16.

9.Malumbres M, Barbacid M. Milestones in cell division: to cycle or not to cycle: a critical decision in cancer. Nature reviews. Cancer. 2001 Dec 1;1(3):222.

10.Malumbres M, Barbacid M. Is Cyclin D1-CDK4 kinase a bona fide cancer target?. Cancer cell. 2006 Jan 31;9(1):2-4.

11.Ruijtenberg S, van den Heuvel S. Coordinating cell proliferation and differentiation: antagonism between cell cycle regulators and cell type-specific gene expression. Cell Cycle. 2016 Jan 17;15(2):196-212.

12.Kandoth C, McLellan MD, Vandin F, Ye K, Niu B, Lu C, Xie M, Zhang Q, McMichael JF, Wyczalkowski MA, Leiserson MD. Mutational landscape and significance across 12 major cancer types. Nature. 2013 Oct 17;502(7471):333.

13.Yu Q, Sicinska E, Geng Y, Ahnström M, Zagozdzon A, Kong Y, Gardner H, Kiyokawa H, Harris LN, Stål O, Sicinski P. Requirement for CDK4 kinase function in breast cancer. Cancer cell. 2006 Jan 31;9(1):23-32.

14.Landis MW, Pawlyk BS, Li T, Sicinski P, Hinds PW. Cyclin D1-dependent kinase activity in murine development and mammary tumorigenesis. Cancer cell. 2006 Jan 31;9(1):13-22.

15.Grillo M, Bott MJ, Khandke N, McGinnis JP, Miranda M, Meyyappan M, Rosfjord EC, Rabindran SK. Validation of cyclin D1/CDK4 as an anticancer drug target in MCF-7 breast cancer cells: effect of regulated overexpression of cyclin D1 and siRNA-mediated inhibition of endogenous cyclin D1 and CDK4 expression. Breast cancer research and treatment. 2006 Jan 1;95(2):185-94.

16.Smith PJ, Yue EW, editors. Inhibitors of cyclin-dependent kinases as anti-tumor agents. CRC Press; 2006 Oct 25.

17.Nugiel DA, Vidwans A, Etzkorn AM, Rossi KA, Benfield PA, Burton CR, Cox S, Doleniak D, Seitz SP. Synthesis and evaluation of indenopyrazoles as cyclin-dependent kinase inhibitors. 2. Probing the indeno ring substituent pattern. Journal of medicinal chemistry. 2002 Nov 21;45(24):5224-32.

18.Mor S, Mohil R, Nagoria S, Kumar A, Lal K, Kumar D, Singh V. Regioselective Synthesis, Antimicrobial Evaluation and QSAR Studies of Some 3-Aryl-1-heteroarylindeno [1, 2-c] pyrazol-4 (1H)-ones. Journal of Heterocyclic Chemistry. 2017 Mar 1;54(2):1327-41.